AIMS Mathematics, 11(1): 2547–2577.
DOI: 10.3934/math.2026103
Received: 29 November 2025
Revised: 11 January 2026
Accepted: 15 January 2026
Published: 26 January 2026

http://www.aimspress.com/journal/Math

Research article

A fractal-fractional perspective on Lassa fever dynamics with saturated incidence and relapse

Sagar R. Khirsariya[1,*] **and Saud Fahad Aldosary**[2]

[1] Department of Mathematics, Marwadi University, Rajkot, Gujarat-360003, India
[2] Department of Mathematics, College of Science and Humanities in Alkharj, Prince Sattam bin Abdulaziz University, Alkharj 11942, Saudi Arabia

* **Correspondence:** Email: ksagar108@gmail.com.

Abstract: This paper presents a comprehensive investigation into the transmission dynamics of Lassa fever through a sophisticated mathematical model formulated with a fractal-fractional operator in the Atangana-Baleanu sense. The model's architecture is an SEIQR (susceptible-exposed-infected-quarantined-recovered) framework that incorporates crucial real-world epidemiological features, including a saturated incidence rate to account for behavioral changes at high infection levels and a relapse mechanism for recovered individuals. A rigorous qualitative analysis is conducted to establish the fundamental properties of the model, wherein we prove the existence, uniqueness, positivity, and boundedness of the solutions, ensuring the biological viability of the system. The stability of the model's equilibria is thoroughly examined. We derive the basic reproduction number (R_0) using a next-generation matrix method, which serves as the critical threshold for disease persistence. We prove that the disease-free equilibrium is both locally and globally asymptotically stable when $R_0 < 1$. For the numerical investigation, we implement and validate a robust predictor-corrector scheme tailored for fractional-order systems, comparing its accuracy and convergence against the fractional Euler method and the classical Runge-Kutta scheme. Extensive numerical simulations are performed to visualize the system's dynamics. The results demonstrate that the fractional order provides enhanced flexibility in capturing memory effects, often leading to a more realistic, delayed epidemic peak. Furthermore, a series of novel three-dimensional dynamic surface plots reveals the geometric sensitivity of the solution manifold to key infection parameters, visually confirming that the transmission rate (β) and quarantine rate (η) are the most powerful levers in shaping the epidemic landscape. These findings offer a deeper understanding of Lassa fever's dynamics and highlight critical points for effective public health interventions.

Keywords: Lassa fever; fractal-fractional calculus; Atangana-Baleanu operator; stability analysis; numerical simulation

Mathematics Subject Classification: 34A08, 34D20, 37N25, 92C50

1. Introduction

Lassa fever, an acute viral hemorrhagic illness, remains a significant public health challenge, particularly in West Africa where it is endemic [1]. The disease is caused by the Lassa virus, a member of the Arenaviridae family, and is primarily transmitted to humans through contact with food or household items contaminated with the excreta of infected *Mastomys* rats [2]. Human-to-human transmission is also possible through direct contact with the blood, urine, feces, or other bodily secretions of an infected person. The clinical presentation of Lassa fever is variable, ranging from asymptomatic infection to severe multi-organ failure and death, with a case fatality rate that can be particularly high in hospitalized patients [3]. The persistent threat and potential for large-scale outbreaks underscore the urgent need for effective control strategies, which can be significantly enhanced by insights from mathematical modeling.

Mathematical models are indispensable tools for understanding the transmission dynamics of infectious diseases and for evaluating the potential impact of public health interventions [4]. Numerous models have been developed to study Lassa fever, exploring various aspects such as rodent-to-human transmission, optimal control strategies, and the role of quarantine [5, 6]. These models have traditionally been formulated using classical integer-order differential equations, which assume that the future state of the system depends only on its current state. However, this assumption may not adequately capture the complexities of biological systems, where memory and hereditary properties can play a crucial role [7]. For instance, the immune response to an infection and the behavioral changes in a population are processes that are influenced by past experiences.

To address these limitations, fractional calculus, which generalizes differentiation and integration to non-integer orders, has emerged as a powerful framework in mathematical epidemiology [8]. Fractional-order models can incorporate memory effects, providing a more realistic description of disease dynamics [7]. Recently, the concept has been further extended to fractal-fractional calculus, which combines the memory-retaining properties of fractional derivatives with the geometric complexity described by fractal dimensions [9]. This dual approach is particularly appealing for modeling infectious diseases, as it can account for both the temporal memory of biological processes and the heterogeneous, fractal-like nature of contact networks within a population [10]. The Atangana-Baleanu (AB) operator, which uses a non-singular Mittag-Leffler kernel, has gained prominence because of its ability to capture complex non-local dynamics without the singularities present in other definitions like the Caputo-Fabrizio operator [11]. This operator has been successfully applied to model various infectious diseases, demonstrating its superiority in fitting real-world data [12, 13].

In recent years, mathematical modeling through fractional-order and fractal-fractional derivatives has gained prominence due to their ability to capture memory effects and complex dynamics in biological systems. Saber and Solouma [14] employed advanced fractional modeling to analyze diabetes via bifurcation and chaos control, while Alhazmi et al. [15] investigated glucose-insulin dynamics using hybrid Euler-Lagrange and successive approximation schemes. The AB operator, characterized by the non-singular Mittag-Leffler kernel, has been successfully applied to model diverse

phenomena such as computer virus networks [16] and pneumonia diseases [17]. Furthermore, hybrid multi-step numerical schemes have been developed for human-wildlife zoonotic disease dynamics to improve computational accuracy [18]. Specific to Lassa fever, recent studies have explored the impact of relapse and saturated incidence rates [19], environmental contamination through optimal control [20], and the influence of treatment compliance on disease spread [21]. These contributions underscore the necessity of employing sophisticated mathematical frameworks, such as fractal-fractional operators, to better understand and control the transmission of Lassa fever.

This manuscript develops and analyzes a Lassa fever model using the Atangana-Baleanu fractal-fractional operator. The model is an extension of the classic susceptible-exposed-infected-recovered (SEIR) framework to an SEIQR structure, incorporating a saturated incidence rate to model the inhibition of disease transmission at high infection levels caused by public awareness or behavioral changes. It also includes a relapse component, allowing individuals in the recovered class to lose immunity and become susceptible again. The primary motivation for using a fractal-fractional approach is to explore how memory and fractal structures influence the transmission dynamics of Lassa fever, potentially offering new insights that are not captured by traditional models.

This paper is organized as follows. Section 2 presents the detailed formulation of the Lassa fever model, including the underlying assumptions and a schematic diagram. Section 3 provides the necessary mathematical preliminaries on fractal-fractional calculus. In Section 4, we conduct a qualitative analysis of the model, proving the existence, uniqueness, positivity, and boundedness of the solutions. Section 5 is dedicated to the stability analysis of the model, including the computation of the basic reproduction number (R_0) and an investigation of the local and global stability of the disease-free and endemic equilibria. Section 6 details the numerical scheme used to solve the fractal-fractional system. Section 7 presents and compares the numerical results obtained using different methods. A comprehensive discussion of the simulation results is provided in Section 8. Finally, Section 9 concludes the paper with a summary of the key findings and directions for future research. Section 10 summarizes the key findings in a table.

2. Model formulation

To investigate the transmission dynamics of Lassa fever, we formulate a deterministic compartmental model. This approach subdivides the total human population, denoted by $N(t)$, into five distinct epidemiological classes based on the disease status of individuals. These compartments are: susceptible ($S(t)$), exposed ($E(t)$), infected ($I(t)$), quarantined ($Q(t)$), and recovered ($R(t)$). The total population is thus the sum of these compartments, $N(t) = S(t)+E(t)+I(t)+Q(t)+R(t)$. The model is constructed as a system of nonlinear ordinary differential equations describing the rate of change of each population over time.

A set of core assumptions underpins the model's structure. We assume a constant recruitment rate into the susceptible population. The transmission of the disease is modeled using a saturated incidence rate, which is more realistic than simple mass action, as it accounts for behavioral changes or saturation effects when the number of infected individuals becomes very high. We also consider that recovered individuals can lose their immunity and become susceptible again, representing a relapse mechanism. Natural death occurs in all compartments at the same rate, whereas the infected class has an additional disease-induced death rate.

The flow of individuals between these compartments is visualized in the schematic diagram shown in Figure 1.

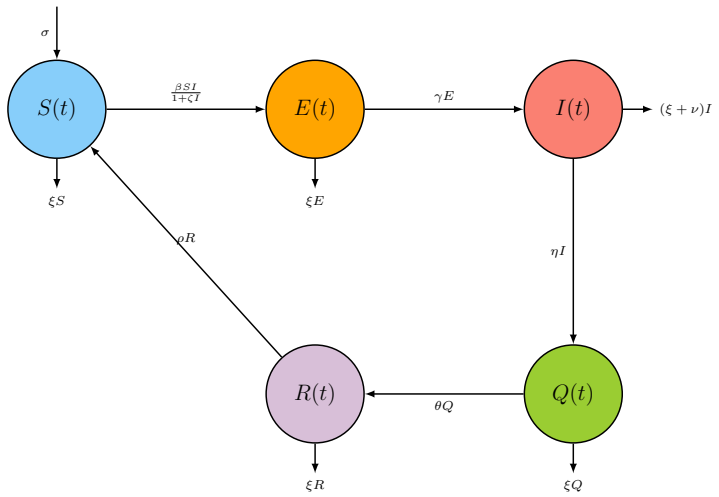

Figure 1. A schematic diagram illustrating the flow between compartments of the Lassa fever transmission model.

The dynamics of the Lassa fever transmission are described by the following system of differential equations:

$$\frac{dS}{dt} = \sigma + \rho R - \frac{\delta S I}{1 + \mu I} - \xi S. \tag{2.1}$$

The change in the susceptible population is governed by four processes. The population increases through a constant recruitment rate, σ, representing births or immigration. This assumption is justified for the 100-day simulation period considered in this study, as demographic changes in the human population occur on a much slower time-scale than the rapid transmission dynamics of a Lassa fever outbreak. It is also increased by individuals from the recovered class, R, who lose their immunity at a rate ρ. The susceptible population decreases when individuals become infected, which is modeled by the saturated incidence term $\frac{\delta S I}{1+\mu I}$. Here, δ is the effective transmission rate. This term approaches a saturation level as the number of infected individuals I grows large, reflecting that the risk of infection does not grow infinitely but is limited by factors such as self-imposed precautions. Finally, the population decreases through to natural death at a rate ξ.

$$\frac{dE}{dt} = \frac{\delta S I}{1 + \mu I} - (\gamma + \xi)E. \tag{2.2}$$

The exposed population, E, consists of individuals who are infected but not yet infectious. This compartment is populated by the newly infected individuals from the susceptible class, as described by the term $\frac{\delta S I}{1+\mu I}$. The population of this class decreases as individuals progress to the infectious state at a rate γ (the term γE) or through natural death at a rate ξ. Thus, the total outflow rate is $(\gamma + \xi)$.

$$\frac{dI}{dt} = \gamma E - (\eta + \xi + \nu)I. \tag{2.3}$$

The infected population, I, comprises individuals who are now capable of transmitting the disease. This class grows as exposed individuals become infectious at a rate γ. The population of the infected class declines for three reasons: Individuals are moved into quarantine at a rate η, they die from natural causes at a rate ξ, or they succumb to the disease at a disease-induced death rate ν. The total rate of removal from this class is therefore $(\eta + \xi + \nu)$.

$$\frac{dQ}{dt} = \eta I - (\theta + \xi)Q. \tag{2.4}$$

The quarantined population, Q, is populated by infected individuals who are isolated at a rate η. The number of quarantined individuals decreases as they recover from the disease at a rate θ or through natural death at a rate ξ. The total outflow rate from this compartment is $(\theta + \xi)$.

$$\frac{dR}{dt} = \theta Q - (\rho + \xi)R. \tag{2.5}$$

The recovered population, R, increases as individuals from the quarantined class recover at a rate θ. This class loses members as individuals lose their immunity and become susceptible again (relapse) at a rate ρ, or through natural death at a rate ξ. The total outflow rate is thus $(\rho + \xi)$.

The parameters used in the model, along with their baseline values sourced from the relevant literature, are summarized in Table 1.

Table 1. Model parameters and their baseline values.

Parameter	Description	Value
σ	Recruitment rate of the population [3]	0.15 day^{-1}
ξ	Natural death rate [2]	0.2 day^{-1}
δ	Effective disease transmission rate [3]	0.008 day^{-1}
γ	Progression rate from exposed to infected [3]	0.5 day^{-1}
μ	Saturation parameter for inhibitory effect [3]	0.03
ν	Disease-induced death rate [2, 3]	0.3 day^{-1}
η	Quarantine rate for infected individuals [3]	0.4 day^{-1}
θ	Recovery rate of quarantined individuals [3]	0.2 day^{-1}
ρ	Rate of immunity loss (relapse) [3]	0.7 day^{-1}

The relapse rate $\rho = 0.7$ day^{-1} (sourced from [3]) represents the reactivation of latent viral infection in individuals who have clinically recovered but still harbor the virus, rather than the loss of long-term sterilizing immunity. This distinction accounts for the relatively high rate observed in short-term Lassa fever dynamics. To better capture the complex memory and hereditary properties inherent in biological systems, we extend the classical integer-order model using the concept of fractal-fractional calculus. This framework allows for a more flexible and realistic description of disease dynamics by incorporating both a fractional order, α, to model memory effects, and a fractal dimension, β, to represent the geometric complexity of the transmission pathways. We use the AB operator because of its non-singular kernel. By replacing the classical integer-order derivative $\frac{d}{dt}$ with the fractal-fractional operator ${}^{AB}D_t^{\alpha,\beta}$, we obtain the following updated system:

$$^{AB}D_t^{\alpha,\beta}S(t) = \sigma + \rho R - \frac{\delta S I}{1+\mu I} - \xi S \tag{2.6}$$

$$^{AB}D_t^{\alpha,\beta}E(t) = \frac{\delta S I}{1+\mu I} - (\gamma + \xi)E \tag{2.7}$$

$$^{AB}D_t^{\alpha,\beta}I(t) = \gamma E - (\eta + \xi + \nu)I \tag{2.8}$$

$$^{AB}D_t^{\alpha,\beta}Q(t) = \eta I - (\theta + \xi)Q \tag{2.9}$$

$$^{AB}D_t^{\alpha,\beta}R(t) = \theta Q - (\rho + \xi)R. \tag{2.10}$$

This fractal-fractional formulation, with $\alpha, \beta \in (0, 1]$, provides the foundation for our subsequent analysis. The fractal-fractional operator generalizes the integer-order model to capture non-local memory (α) and self-similar scaling (β). This transformation is justified by the non-Markovian nature of Lassa fever's transmission, where the epidemic's growth follows a power-law rather than exponential dynamics.

The proposed SEIQR structure is specifically tailored to Lassa fever's epidemiology. The *quarantined* (Q) class is included to account for the rigorous isolation protocols required to prevent nosocomial transmission, a major driver of Lassa outbreaks. Furthermore, the *saturated incidence* rate $\frac{\beta S I}{1+\zeta I}$ models the reduction in human-to-human and rodent-to-human contact resulting from public health awareness and behavioral changes (e.g., improved food storage and hygiene) during an epidemic. The *relapse* mechanism reflects the potential for waning immunity or re-infection in endemic regions where the Lassa virus persists in rodent reservoirs.

Recovery is assumed to occur exclusively through the quarantined (Q) class to reflect the clinical management of Lassa fever. This structural choice signifies that symptomatic individuals in the community (I) are either isolated for specialized treatment or remain infectious until they are quarantined or succumb to the disease, emphasizing the role of the healthcare system in achieving safe recovery.

3. Preliminaries

In this section, we provide the fundamental definitions of the AB fractional and fractal-fractional operators that are used in this study.

Definition 3.1 (AB fractional derivative in Caputo sense [11]). *Let $f \in H^1(a, b)$, $b > a$, and $\alpha \in (0, 1]$. The AB fractional derivative in the Caputo (ABC) sense is defined as*

$$^{ABC}D_t^{\alpha} f(t) = \frac{B(\alpha)}{1-\alpha} \int_a^t f'(\tau) E_\alpha \left(-\frac{\alpha}{1-\alpha}(t-\tau)^\alpha \right) d\tau,$$

where $B(\alpha)$ is a normalization function such that $B(0) = B(1) = 1$, and E_α is the one-parameter Mittag-Leffler function defined as:

$$E_\alpha(z) = \sum_{k=0}^{\infty} \frac{z^k}{\Gamma(\alpha k + 1)}.$$

Remark 3.2. *The inclusion of $\alpha = 1$ in the interval $(0, 1]$ signifies the limiting case of the operator. As $\alpha \to 1$, the kernel of the fractional derivative converges to a Dirac delta function, and the operator reduces to the classical integer-order derivative.*

Definition 3.3 (AB fractional integral [11]). *The corresponding AB fractional integral is defined as*

$$^{AB}I_t^{\alpha} f(t) = \frac{1-\alpha}{B(\alpha)} f(t) + \frac{\alpha}{B(\alpha)\Gamma(\alpha)} \int_a^t f(\tau)(t-\tau)^{\alpha-1} d\tau.$$

The concept was extended to fractal-fractional derivatives by incorporating a fractal dimension β.

Definition 3.4 (Fractal-fractional derivative in AB sense [9]). *Let $f(t)$ be a continuous function. The fractal-fractional derivative of order α and the fractal dimension β in the AB sense is defined as*

$$^{AB}D_t^{\alpha,\beta} f(t) = \frac{B(\alpha)}{1-\alpha} \int_0^t \frac{d}{d\tau^{\beta}} f(\tau) E_{\alpha}\left(-\frac{\alpha}{1-\alpha}(t-\tau)^{\alpha}\right) d\tau,$$

where $\frac{d}{d\tau^{\beta}} f(\tau) = \lim_{t\to\tau} \frac{f(t)-f(\tau)}{t^{\beta}-\tau^{\beta}}$. This can be simplified for practical applications by writing $\frac{df(\tau)}{d\tau^{\beta}} = \tau^{1-\beta}\frac{df(\tau)}{d\tau}$. This leads to the following more tractable form:

$$^{AB}D_t^{\alpha,\beta} f(t) = \frac{B(\alpha)}{1-\alpha} \int_0^t \tau^{1-\beta} f'(\tau) E_{\alpha}\left(-\frac{\alpha}{1-\alpha}(t-\tau)^{\alpha}\right) d\tau.$$

The corresponding fractal-fractional integral is given by applying the AB fractional integral operator to the function $t^{\beta-1} f(t)$.

Lemma 3.5. *The fractal-fractional differential equation $^{AB}D_t^{\alpha,\beta} y(t) = g(t, y(t))$ with the initial condition $y(0) = y_0$ can be transformed into the following equivalent Volterra integral equation:*

$$y(t) - y_0 = \frac{1-\alpha}{B(\alpha)} t^{\beta-1} g(t, y(t)) + \frac{\alpha}{B(\alpha)\Gamma(\alpha)} \int_0^t (t-\tau)^{\alpha-1} \tau^{\beta-1} g(\tau, y(\tau)) d\tau.$$

4. Qualitative analysis of the model

This section is dedicated to the rigorous mathematical analysis of the proposed fractal-fractional Lassa fever model given by Eqs (2.6)–(2.10). To ensure that the model is epidemiologically and mathematically well-posed, we must establish several fundamental properties of its solutions. Specifically, we will prove the existence and uniqueness of the solution, confirm that the solution remains non-negative (positivity), and demonstrate that the solution is bounded within a biologically feasible region. These properties guarantee that the model's predictions are meaningful and stable over time.

For clarity, let us represent the state variables as a vector $Y(t) = (S(t), E(t), I(t), Q(t), R(t))^T$. The system of fractal-fractional differential equations can be expressed in a compact as follows

$$^{AB}D_t^{\alpha,\beta} Y(t) = F(t, Y(t)), \text{ with initial condition } Y(0) = Y_0 \geq 0,$$

where $F : \mathbb{R}_+^5 \to \mathbb{R}^5$ is a vector function representing the right-hand sides of the model equations. Our analysis will rely on transforming this system into an equivalent Volterra integral equation, upon which we can apply principles from fixed-point theory.

4.1. Existence and uniqueness of the solution

We will use the framework of Banach spaces and the well-established Banach fixed-point theorem to demonstrate the existence and uniqueness of the solution. The first crucial step is to show that the function $F(t, Y(t))$, which defines the dynamics of our system, satisfies the Lipschitz condition.

Theorem 4.1 (Lipschitz condition)**.** *The kernel $F(t, Y)$ satisfies the Lipschitz condition with respect to Y if a constant $L > 0$ exist such that for any two state vectors $Y(t)$ and $Y^*(t)$ in a subset of $\mathbb{R}^5_+$, the following inequality holds:*

$$\|F(t, Y) - F(t, Y^*)\| \leq L\|Y - Y^*\|.$$

Proof. Let $Y = (S, E, I, Q, R)^T$ and $Y^* = (S^*, E^*, I^*, Q^*, R^*)^T$ be two distinct state vectors. The components of F are F_S, F_E, F_I, F_Q, F_R. Let us analyze the first component, F_S as follows

$$F_S(t, Y) - F_S(t, Y^*) = (\sigma + \rho R - \tfrac{\delta S I}{1+\mu I} - \xi S) - (\sigma + \rho R^* - \tfrac{\delta S^* I^*}{1+\mu I^*} - \xi S^*)$$

$$= \rho(R - R^*) - \xi(S - S^*) - \beta\left(\tfrac{S I}{1+\mu I} - \tfrac{S^* I^*}{1+\mu I^*}\right).$$

Since the solution is bounded (as we will prove later), we can assume there is a constant $M_I > 0$ such that $I \leq M_I$. The saturated incidence function $g(S, I) = \frac{S I}{1+\mu I}$ is continuously differentiable in the feasible region, and its partial derivatives are bounded. Therefore, it is Lipschitz. For simplicity, we can bound the difference as follows:

$$\left\|\tfrac{S I}{1+\mu I} - \tfrac{S^* I^*}{1+\mu I^*}\right\| \leq C_1\|S - S^*\| + C_2\|I - I^*\| \text{ for some positive constants } C_1, C_2.$$

Taking the norm, we get:

$$\|F_S(t, Y) - F_S(t, Y^*)\| \leq \rho\|R - R^*\| + \xi\|S - S^*\| + \beta(C_1\|S - S^*\| + C_2\|I - I^*\|)$$

$$\leq (\xi + \beta C_1)\|S - S^*\| + \beta C_2\|I - I^*\| + \rho\|R - R^*\|.$$

A similar procedure can be applied to the other components of F as follows

$$\|F_E(t, Y) - F_E(t, Y^*)\| \leq (\gamma + \xi)\|E - E^*\| + \beta(C_1\|S - S^*\| + C_2\|I - I^*\|)$$

$$\|F_I(t, Y) - F_I(t, Y^*)\| \leq \gamma\|E - E^*\| + (\eta + \xi + \nu)\|I - I^*\|$$

$$\|F_Q(t, Y) - F_Q(t, Y^*)\| \leq \eta\|I - I^*\| + (\theta + \xi)\|Q - Q^*\|$$

$$\|F_R(t, Y) - F_R(t, Y^*)\| \leq \theta\|Q - Q^*\| + (\rho + \xi)\|R - R^*\|.$$

By summing the inequalities and choosing an appropriate maximum of the coefficients, we can find a constant $L > 0$ such that $\|F(t, Y) - F(t, Y^*)\| \leq L\|Y - Y^*\|$. Thus, the kernel F satisfies the Lipschitz condition. □

With the Lipschitz condition established, we can now prove the main theorem for existence and uniqueness.

Theorem 4.2 (Existence and uniqueness)**.** *For the given initial conditions $Y_0 \geq 0$, a unique solution for the fractal-fractional system (2.6)–(2.10) exists for $t \in [0, T]$ for some $T > 0$.*

Proof. The proof relies on converting the system of differential equations into a system of Volterra integral equations and then applying the Banach fixed-point theorem [22]. The integral form of the system is

$$Y(t) = Y(0) + \frac{1-\alpha}{B(\alpha)} t^{\beta-1} F(t, Y(t)) + \frac{\alpha}{B(\alpha)\Gamma(\alpha)} \int_0^t (t-\tau)^{\alpha-1} \tau^{\beta-1} F(\tau, Y(\tau)) d\tau.$$

Let us define an operator $\mathcal{P}$ on the Banach space of continuous functions $C[0, T]$ as follows

$$(\mathcal{P}Y)(t) = Y(0) + \frac{1-\alpha}{B(\alpha)} t^{\beta-1} F(t, Y(t)) + \frac{\alpha}{B(\alpha)\Gamma(\alpha)} \int_0^t (t-\tau)^{\alpha-1} \tau^{\beta-1} F(\tau, Y(\tau)) d\tau.$$

A solution to the system is a fixed point of the operator $\mathcal{P}$, i.e., $\mathcal{P}Y = Y$. We need to show that $\mathcal{P}$ is a contraction mapping. Let Y and Y^* be two functions in the Banach space.

$$\|(\mathcal{P}Y)(t) - (\mathcal{P}Y^*)(t)\| \leq \frac{1-\alpha}{B(\alpha)} t^{\beta-1} \|F(t, Y) - F(t, Y^*)\|$$

$$+ \frac{\alpha}{B(\alpha)\Gamma(\alpha)} \int_0^t (t-\tau)^{\alpha-1} \tau^{\beta-1} \|F(\tau, Y) - F(\tau, Y^*)\| d\tau.$$

Using the Lipschitz condition, $\|F(t, Y) - F(t, Y^*)\| \leq L\|Y - Y^*\|$, we have

$$\|(\mathcal{P}Y)(t) - (\mathcal{P}Y^*)(t)\| \leq \frac{(1-\alpha)L}{B(\alpha)} T^{\beta-1} \|Y - Y^*\|$$

$$+ \frac{\alpha L}{B(\alpha)\Gamma(\alpha)} \|Y - Y^*\| \int_0^t (t-\tau)^{\alpha-1} \tau^{\beta-1} d\tau.$$

The integral evaluates to $t^{\alpha+\beta-1} B(\alpha, \beta)$, where B is the beta function. Thus, we have

$$\|(\mathcal{P}Y)(t) - (\mathcal{P}Y^*)(t)\| \leq \left(\frac{(1-\alpha)LT^{\beta-1}}{B(\alpha)} + \frac{\alpha L T^{\alpha+\beta-1} B(\alpha,\beta)}{B(\alpha)\Gamma(\alpha)} \right) \|Y - Y^*\|.$$

Let $\Lambda = \left(\frac{(1-\alpha)LT^{\beta-1}}{B(\alpha)} + \frac{\alpha L T^{\alpha+\beta-1} B(\alpha,\beta)}{B(\alpha)\Gamma(\alpha)} \right)$. For a sufficiently small time T, we can ensure that $\Lambda < 1$. When $\Lambda < 1$, the operator $\mathcal{P}$ is a contraction mapping. By the Banach fixed-point theorem, $\mathcal{P}$ has a unique fixed point, which corresponds to the unique solution of our system on the interval $[0, T]$. This local solution can be extended to a global one. □

4.2. Positivity of solutions

For the model to be epidemiologically meaningful, all state variables must remain non-negative for all times $t \geq 0$. We prove this property in the following theorem.

Theorem 4.3. *(Positivity). Given the non-negative initial conditions* $(S(0), E(0), I(0), Q(0), R(0)) \in \mathbb{R}^5_+$*, the solution* $(S(t), E(t), I(t), Q(t), R(t))$ *of the fractal-fractional system (2.6)–(2.10) remains non-negative for all* $t \geq 0$*.*

Proof. Suppose that the initial conditions are non-negative. To prove that the solutions stay in the first orthant $\mathbb{R}^5_+$, we define t^* as the first time any of the state variables reaches zero

$$t^* = \inf\{t > 0 : \min(S(t), E(t), I(t), Q(t), R(t)) = 0\}.$$

By this definition, for all $t \in [0, t^*]$, all state variables are non-negative ($S, E, I, Q, R \geq 0$). We now examine the behavior of the system at $t = t^*$.

- **Case 1:** $S(t^*) = 0$. From the first equation of the system (2.6), we have

$$^{AB}D_t^{\alpha\beta}S(t)|_{t=t^*} = \sigma + \rho R(t^*) - \frac{\delta S(t^*)I(t^*)}{1+\mu I(t^*)} - \xi S(t^*).$$

  Substituting $S(t^*) = 0$, we obtain

$$^{AB}D_t^{\alpha\beta}S(t)|_{t=t^*} = \sigma + \rho R(t^*).$$

  Since $\sigma > 0$ and $R(t^*) \geq 0$ (by the definition of t^*), it follows that $^{AB}D_t^{\alpha\beta}S(t)|_{t=t^*} > 0$.

- **Case 2:** $E(t^*) = 0$. From Eq (2.7), we have

$$^{AB}D_t^{\alpha\beta}E(t)|_{t=t^*} = \frac{\delta S(t^*)I(t^*)}{1+\mu I(t^*)} - (\gamma+\xi)E(t^*) = \frac{\delta S(t^*)I(t^*)}{1+\mu I(t^*)} \geq 0$$

  as $S(t^*) \geq 0$ and $I(t^*) \geq 0$.

- **Case 3:** $I(t^*) = 0$. From Eq (2.8), we have

$$^{AB}D_t^{\alpha\beta}I(t)|_{t=t^*} = \gamma E(t^*) - (\eta+\xi+\nu)I(t^*) = \gamma E(t^*) \geq 0,$$

  as $E(t^*) \geq 0$.

- **Case 4:** $Q(t^*) = 0$. From Eq (2.9), we have

$$^{AB}D_t^{\alpha\beta}Q(t)|_{t=t^*} = \eta I(t^*) - (\theta+\xi)Q(t^*) = \eta I(t^*) \geq 0,$$

  as $I(t^*) \geq 0$.

- **Case 5:** $R(t^*) = 0$. From Eq (2.10), we have

$$^{AB}D_t^{\alpha\beta}R(t)|_{t=t^*} = \theta Q(t^*) - (\rho+\xi)R(t^*) = \theta Q(t^*) \geq 0,$$

  as $Q(t^*) \geq 0$.

Since the fractal-fractional derivative of the variable reaching zero is always non-negative (and strictly positive for S), the variables cannot cross into the negative region. Thus, the solution remains in $\mathbb{R}^5_+$ for all $t \geq 0$. □

4.3. Boundedness of the solutions

Finally, we must show that the total population in the model does not grow without limit. This confirms that the model is well-posed and that the disease dynamics occur within a defined, biologically feasible region.

Theorem 4.4 (Boundedness)**.** *All solutions of the fractal-fractional system that start in the non-negative orthant $\mathbb{R}^5_+$ are bounded and ultimately enter the feasible region Ω defined by:*

$$\Omega = \left\{(S,E,I,Q,R) \in \mathbb{R}^5_+ : S+E+I+Q+R \leq \tfrac{\sigma}{\xi}\right\}.$$

Proof. Let $N(t)$ represent the total population at time t, such that $N(t) = S(t) + E(t) + I(t) + Q(t) + R(t)$. We take the fractal-fractional derivative of $N(t)$ by summing the equations in the model system (2.6)–(2.10):

$$^{AB}D_t^{\alpha,\beta}N(t) = {}^{AB}D_t^{\alpha,\beta}S(t) + {}^{AB}D_t^{\alpha,\beta}E(t) + {}^{AB}D_t^{\alpha,\beta}I(t) + {}^{AB}D_t^{\alpha,\beta}Q(t) + {}^{AB}D_t^{\alpha,\beta}R(t).$$

Substituting the right-hand sides of the model equations and simplifying, we obtain:

$$^{AB}D_t^{\alpha,\beta}N(t) = \left(\sigma + \rho R - \tfrac{\delta SI}{1+\mu I} - \xi S\right) + \left(\tfrac{\delta SI}{1+\mu I} - (\gamma + \xi)E\right)$$

$$+ (\gamma E - (\eta + \xi + \nu)I) + (\eta I - (\theta + \xi)Q) + (\theta Q - (\rho + \xi)R).$$

Many terms cancel out, leaving:

$$^{AB}D_t^{\alpha,\beta}N(t) = \sigma - \xi S - \xi E - \xi I - \xi Q - \xi R - \nu I$$

$$^{AB}D_t^{\alpha,\beta}N(t) = \sigma - \xi(S + E + I + Q + R) - \nu I$$

$$^{AB}D_t^{\alpha,\beta}N(t) = \sigma - \xi N(t) - \nu I(t).$$

Since the infected population $I(t)$ is non-negative, the term $-\nu I(t)$ is always less than or equal to zero. Therefore, we can establish the following inequality:

$$^{AB}D_t^{\alpha,\beta}N(t) \leq \sigma - \xi N(t).$$

Consider the case where $N(t) > \frac{\sigma}{\xi}$. In this scenario, $\sigma - \xi N(t) < 0$, which implies that $^{AB}D_t^{\alpha,\beta}N(t) < 0$. This means that the total population $N(t)$ will decrease whenever it exceeds the value $\frac{\sigma}{\xi}$. According to the comparison theorem for fractional differential inequalities [23], the solution $N(t)$ is bounded above by the solution to the equation $^{AB}D_t^{\alpha,\beta}Z(t) = \sigma - \xi Z(t)$ with $Z(0) = N(0)$, which converges to the equilibrium point $Z_{eq} = \frac{\sigma}{\xi}$. Therefore, for any non-negative initial condition, the total population $N(t)$ will not grow indefinitely and will eventually enter and remain within the region Ω. This confirms that the model is biologically consistent. □

Following the proofs of existence and uniqueness in Sections 4.1 and 4.2, and the establishment of positivity and boundedness in the last section, the proposed fractal-fractional Lassa fever model is mathematically and biologically well-posed within the invariant region Ω. This ensures that the system's solutions are globally defined, unique, and physically meaningful.

5. Stability analysis

The stability analysis of an epidemiological model is paramount, as it determines the conditions under which a disease will either die out or persist within a population. This section investigates the stability of the equilibrium points of the Lassa fever model. An equilibrium point is a state where the populations of all compartments remain constant over time. We will identify two key equilibria: The disease-free equilibrium (DFE), where the disease is absent, and the endemic equilibrium (EE), where the disease is maintained in the population. Our analysis is structured in two parts: Local stability, which describes the system's behavior near an equilibrium point, and global stability, which describes the system's long-term behavior across the entire feasible region.

5.1. Local asymptotic stability

Local stability is assessed by linearizing the system around its equilibrium points. The cornerstone of this analysis is the basic reproduction number, R_0.

5.1.1. Disease-free equilibrium and the basic reproduction number (R_0)

The DFE is the state where there are no infected individuals in the population. To find the DFE, we set the right-hand sides of the model equations to zero, with the condition that $E = I = Q = R = 0$. From the equation for the susceptible class, we have

$$\frac{dS}{dt} = \sigma - \xi S = 0 \implies S = \frac{\sigma}{\xi}.$$

Thus, the DFE point, denoted by E_0, is given by:

$$E_0 = (S^0, E^0, I^0, Q^0, R^0) = \left(\frac{\sigma}{\xi}, 0, 0, 0, 0\right).$$

The basic reproduction number, R_0, is defined as the average number of secondary infections produced by a single infected individual introduced into a completely susceptible population. We compute R_0 using the next-generation matrix method as outlined in [24]. We consider only the compartments of infected individuals, which are E and I. Let $\mathcal{F}$ be the vector of new infection rates and $\mathcal{V}$ be the vector of the transfer rates between these compartments.

$$\mathcal{F} = \begin{pmatrix} \frac{\delta S I}{1+\mu I} \\ 0 \end{pmatrix}, \quad \mathcal{V} = \begin{pmatrix} (\gamma + \xi)E \\ -\gamma E + (\eta + \xi + \nu)I \end{pmatrix}.$$

Next, we compute the Jacobian matrices of $\mathcal{F}$ and $\mathcal{V}$ evaluated at the DFE, E_0. Let these be F and V.

$$F = \frac{\partial \mathcal{F}}{\partial (E,I)}\bigg|_{E_0} = \begin{pmatrix} 0 & \frac{\delta S^0}{(1+\mu\cdot 0)^2} \\ 0 & 0 \end{pmatrix} = \begin{pmatrix} 0 & \frac{\delta\sigma}{\xi} \\ 0 & 0 \end{pmatrix}$$

$$V = \frac{\partial \mathcal{V}}{\partial (E,I)}\bigg|_{E_0} = \begin{pmatrix} \gamma + \xi & 0 \\ -\gamma & \eta + \xi + \nu \end{pmatrix}.$$

The next-generation matrix is given by $K = FV^{-1}$. The inverse of V is

$$V^{-1} = \frac{1}{(\gamma+\xi)(\eta+\xi+\nu)} \begin{pmatrix} \eta + \xi + \nu & 0 \\ \gamma & \gamma + \xi \end{pmatrix}.$$

Therefore, the next-generation matrix K is

$$K = FV^{-1} = \begin{pmatrix} \frac{\delta\sigma\gamma}{\xi(\gamma+\xi)(\eta+\xi+\nu)} & \frac{\delta\sigma(\gamma+\xi)}{\xi(\gamma+\xi)(\eta+\xi+\nu)} \\ 0 & 0 \end{pmatrix}.$$

The basic reproduction number, R_0, is the spectral radius (the largest eigenvalue) of the matrix K.

$$R_0 = \rho(K) = \frac{\delta\sigma\gamma}{\xi(\gamma + \xi)(\eta + \xi + \nu)}. \tag{5.1}$$

Remark 5.1. *Although individuals in the Q (quarantined) compartment are infected, they are excluded from the calculation of the basic reproduction number R_0 and the construction of the Lyapunov function. This is because Q represents individuals who are isolated and under medical supervision, meaning they have no contact with the susceptible population S and thus do not contribute to the generation of new infections. Mathematically, the Q and R compartments act as "sink" or "downstream" variables that do not drive the epidemic's growth; their stability is a direct consequence of the extinction of the infectious classes E and I.*

Remark 5.2. *It is important to note that the basic reproduction number R_0 is a threshold parameter derived from the linearization of the system at the DFE. In fractal-fractional systems, while the operators α and β introduce memory effects and time-scaling ($t^{\beta-1}$), they do not alter the algebraic structure of the DFE or the Jacobian matrices F and V. Consequently, R_0 remains invariant across integer and fractal-fractional orders, as it determines the boundary of stability rather than the transient speed of the epidemic's spread.*

Theorem 5.3 (Local stability of the DFE)**.** *The DFE (E_0) of the Lassa fever model is locally asymptotically stable if $R_0 < 1$, and it is unstable if $R_0 > 1$.*

Proof. The local stability of an equilibrium point is determined by the eigenvalues of the Jacobian matrix of the system evaluated at that point. For a fractional-order system, the equilibrium is stable if all eigenvalues λ_i satisfy the condition $|\arg(\lambda_i)| > \alpha\pi/2$. This condition is met if all eigenvalues have negative real parts [25]. The Jacobian matrix of the full system at a general point (S, E, I, Q, R) is

$$J = \begin{pmatrix} -\frac{\delta I}{1+\mu I} - \xi & 0 & -\frac{\delta S}{(1+\mu I)^2} & 0 & \rho \\ \frac{\delta I}{1+\mu I} & -(\gamma+\xi) & \frac{\delta S}{(1+\mu I)^2} & 0 & 0 \\ 0 & \gamma & -(\eta+\xi+\nu) & 0 & 0 \\ 0 & 0 & \eta & -(\theta+\xi) & 0 \\ 0 & 0 & 0 & \theta & -(\rho+\xi) \end{pmatrix}.$$

Evaluating this matrix at the DFE, $E_0 = (\frac{\sigma}{\xi}, 0, 0, 0, 0)$, we get:

$$J(E_0) = \begin{pmatrix} -\xi & 0 & -\frac{\delta\sigma}{\xi} & 0 & \rho \\ 0 & -(\gamma+\xi) & \frac{\delta\sigma}{\xi} & 0 & 0 \\ 0 & \gamma & -(\eta+\xi+\nu) & 0 & 0 \\ 0 & 0 & \eta & -(\theta+\xi) & 0 \\ 0 & 0 & 0 & \theta & -(\rho+\xi) \end{pmatrix}.$$

The eigenvalues of this block-triangular matrix are the eigenvalues of its diagonal blocks. We can immediately identify three real, negative eigenvalues from the diagonal: $\lambda_1 = -\xi$, $\lambda_2 = -(\theta+\xi)$, and $\lambda_3 = -(\rho+\xi)$. The stability is therefore determined by the eigenvalues of the remaining 2×2 submatrix related to the infectious compartments

$$J_{inf} = \begin{pmatrix} -(\gamma+\xi) & \frac{\delta\sigma}{\xi} \\ \gamma & -(\eta+\xi+\nu) \end{pmatrix}.$$

The eigenvalues of J_{inf} are the roots of its characteristic equation: $\lambda^2 - \mathrm{Tr}(J_{inf})\lambda + \det(J_{inf}) = 0$. The trace is $\mathrm{Tr}(J_{inf}) = -(\gamma+\xi) - (\eta+\xi+\nu)$, which is always negative. The determinant is $\det(J_{inf}) = (\gamma+\xi)(\eta+\xi+\nu) - \gamma\frac{\delta\sigma}{\xi}$. We can rewrite the determinant in terms of R_0 as follows:

$$\det(J_{inf}) = (\gamma+\xi)(\eta+\xi+\nu)\left(1-\frac{\delta\sigma\gamma}{\xi(\gamma+\xi)(\eta+\xi+\nu)}\right) = (\gamma+\xi)(\eta+\xi+\nu)(1-R_0).$$

According to the Routh-Hurwitz criterion, the roots of the characteristic equation will have negative real parts if and only if the trace is negative and the determinant is positive. Since $\mathrm{Tr}(J_{inf}) < 0$, the stability condition reduces to requiring $\det(J_{inf}) > 0$. This inequality holds if and only if $1 - R_0 > 0$, which means that $R_0 < 1$. If $R_0 > 1$, the determinant becomes negative, leading to one positive eigenvalue, which makes the DFE unstable. Therefore, the DFE is locally asymptotically stable for $R_0 < 1$. □

Discussion: As illustrated in Figure 2, when the basic reproduction number R_0 is less than unity, the disease dies out over time. Conversely, for $R_0 > 1$, the infected population does not vanish but instead persists at a steady state, confirming the existence and stability of the EE as derived in Section 5.

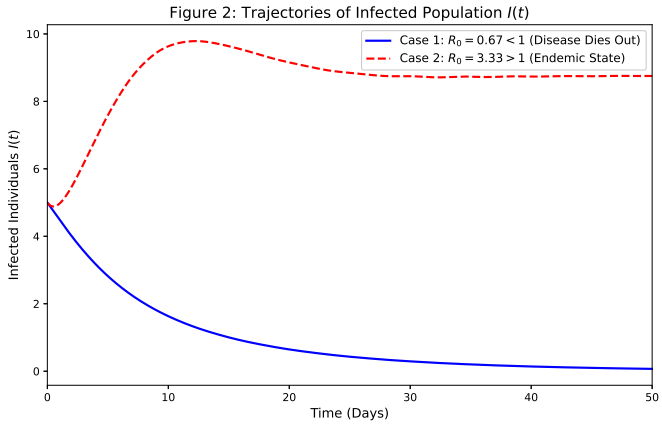

Figure 2. Numerical simulation of the infected population $I(t)$ for different values of R_0. Case 1: $R_0 = 0.67 < 1$ (blue solid line) shows the system converging to the DFE. Case 2: $R_0 = 3.33 > 1$ (red dashed line) shows the population stabilizing at the EE point.

5.1.2. Endemic equilibrium and local stability

The EE $E^* = (S^*, E^*, I^*, Q^*, R^*)$ is obtained by setting Eqs (2.6)–(2.10) to zero. The components are given by

$$S^* = \frac{C(1+\mu I^*)}{\beta}, \quad E^* = \frac{(\eta+\xi+\nu)I^*}{\gamma}, \quad Q^* = \frac{\eta I^*}{\theta+\xi}, \quad R^* = \frac{\eta\theta I^*}{(\theta+\xi)(\rho+\xi)}, \tag{5.2}$$

where $C = \frac{(\gamma+\xi)(\eta+\xi+\nu)}{\gamma}$ and I^* is

$$I^* = \frac{\sigma(1-1/R_0)}{C + \frac{\mu\xi C}{\beta} - \frac{\rho\theta\eta}{(\theta+\xi)(\rho+\xi)}}. \tag{5.3}$$

The local stability of E^* is determined by the Jacobian matrix $J(E^*)$:

$$J(E^*) = \begin{pmatrix} -(\lambda^*+\xi) & 0 & -\frac{\delta S^*}{(1+\mu I^*)^2} & 0 & \rho \\ \lambda^* & -(\gamma+\xi) & \frac{\delta S^*}{(1+\mu I^*)^2} & 0 & 0 \\ 0 & \gamma & -(\eta+\xi+\nu) & 0 & 0 \\ 0 & 0 & \eta & -(\theta+\xi) & 0 \\ 0 & 0 & 0 & \theta & -(\rho+\xi) \end{pmatrix} \tag{5.4}$$

where $\lambda^* = \frac{\delta I^*}{1+\mu I^*}$. E^* is locally asymptotically stable if $R_0 > 1$, as confirmed by the Routh-Hurwitz criteria applied to the characteristic polynomial of $J(E^*)$.

5.2. Global asymptotic stability

Global stability analysis determines the long-term behavior of the system from any initial condition within the feasible region. Here, we focus on the global stability of the DFE.

Lemma 5.4 (LaSalle's invariance principle for fractal-fractional AB systems)**.** *Let $\Omega \subset \mathbb{R}^n$ be a compact set that is positively invariant with respect to the fractal-fractional system. Let $V(x) : \Omega \to \mathbb{R}$ be a continuously differentiable function such that the fractal-fractional derivative satisfies ${}^{FF}D_t^{\alpha,\beta}V(x) \leq 0$ for all $x \in \Omega$. Let $E = \{x \in \Omega : {}^{FF}D_t^{\alpha,\beta}V(x) = 0\}$ and M be the largest invariant set in E. Then every solution starting in Ω approaches M as $t \to \infty$ [26].*

Theorem 5.5 (Global stability of the DFE)**.** *If the basic reproduction number $R_0 \leq 1$, the DFE (E_0) is globally asymptotically stable in the feasible region Ω.*

Proof. To prove the global stability of the DFE, we construct a suitable Lyapunov function $L(S, E, I, Q, R)$ and apply LaSalle's invariance principle for fractional-order systems [27]. Let us define a linear Lyapunov function focused on the infected compartments as follows

$$L(t) = aE(t) + I(t),$$

where a is a positive constant to be determined. The function L is positive definite with respect to the infected states. We now evaluate the fractal-fractional derivative of $L(t)$ along the solution trajectories of the model.

$$\begin{aligned} {}^{AB}D_t^{\alpha,\beta}L(t) &= a\left({}^{AB}D_t^{\alpha,\beta}E(t)\right) + {}^{AB}D_t^{\alpha,\beta}I(t), \\ &= a\left(\frac{\delta S I}{1+\mu I} - (\gamma+\xi)E\right) + (\gamma E - (\eta+\xi+\nu)I). \end{aligned}$$

Since all solutions are bounded within the region Ω, we know that $S(t) \leq S^0 = \frac{\sigma}{\xi}$. Moreover, for any $I > 0$, the term $\frac{1}{1+\mu I} < 1$. Thus, we can write the inequality:

$${}^{AB}D_t^{\alpha,\beta}L(t) \leq a\delta S^0 I - a(\gamma+\xi)E + \gamma E - (\eta+\xi+\nu)I.$$

Grouping terms by E and I, we have

$${}^{AB}D_t^{\alpha,\beta}L(t) \leq (\gamma - a(\gamma+\xi))E + (a\delta S^0 - (\eta+\xi+\nu))I.$$

Our goal is to choose the constant a such that the coefficients of E and I are non-positive. Let us choose a to make the coefficient of E equal to zero, as follows:

$$\gamma - a(\gamma+\xi) = 0 \implies a = \frac{\gamma}{\gamma+\xi}.$$

Since γ and ξ are positive, a is also positive. We now substitute this value of a into the coefficient of I as follows

$$a\delta S^0 - (\eta+\xi+\nu) = \left(\frac{\gamma}{\gamma+\xi}\right)\delta\left(\frac{\sigma}{\xi}\right) - (\eta+\xi+\nu)$$

$$= \frac{\delta\sigma\gamma}{\xi(\gamma+\xi)} - (\eta+\xi+\nu)$$
$$= (\eta+\xi+\nu)\left(\frac{\delta\sigma\gamma}{\xi(\gamma+\xi)(\eta+\xi+\nu)} - 1\right)$$
$$= (\eta+\xi+\nu)(R_0-1).$$

Substituting this back into the inequality for the derivative of $L(t)$, we have

$${}^{AB}D_t^{\alpha,\beta}L(t) \leq (\eta+\xi+\nu)(R_0-1)I(t).$$

If $R_0 \leq 1$, then $(R_0-1) \leq 0$. Since all the other terms are positive, we have ${}^{AB}D_t^{\alpha,\beta}L(t) \leq 0$. The derivative is equal to zero only if $R_0 = 1$ or if $I(t) = 0$. If $I(t) = 0$ for all t, the system's equations imply that $E(t)$ must also approach zero. The largest invariant set in Ω where ${}^{AB}D_t^{\alpha,\beta}L(t) = 0$ is the singleton set $\{E_0\}$. By LaSalle's invariance principle, every solution starting in Ω must converge to E_0 as $t \to \infty$. Thus, the DFE is globally asymptotically stable when $R_0 \leq 1$. □

6. Numerical solution and methodology

To explore the complex dynamics of the fractal-fractional Lassa fever model defined by Eqs (2.6)–(2.10), we require a robust numerical scheme capable of accurately approximating the solutions. Standard solvers for ordinary differential equations are not suitable for systems involving fractal-fractional operators because of their non-local nature, which requires accounting for the entire history of the solution at each time step.

In this section, we detail a powerful and widely-used numerical approach: The predictor-corrector method, also known as the fractional Adams-Bashforth-Moulton method. This technique is well-suited for such problems, as it offers a good balance between computational efficiency and accuracy. We will first provide a thorough derivation of the general methodology and then apply it to construct an iterative scheme for our specific Lassa fever model.

6.1. Derivation of the predictor-corrector scheme

Our goal is to solve a general fractal-fractional initial value problem of the following

$${}^{AB}D_t^{\alpha,\beta}y(t) = f(t,y(t)), \quad y(0) = y_0, \tag{6.1}$$

where ${}^{AB}D_t^{\alpha,\beta}$ is the AB operator. The first step in developing a numerical scheme is to convert this differential equation into an equivalent Volterra integral equation. Applying the corresponding fractal-fractional integral operator to both sides of Eq (6.1) yields:

$$y(t) = y_0 + \frac{1-\alpha}{B(\alpha)}t^{\beta-1}f(t,y(t)) + \frac{\alpha}{B(\alpha)\Gamma(\alpha)}\int_0^t (t-\tau)^{\alpha-1}\tau^{\beta-1}f(\tau,y(\tau))d\tau, \tag{6.2}$$

where $B(\alpha)$ is the normalization function, typically assumed to be 1. We discretize the time interval $[0,T]$ into N subintervals of equal width h, such that $t_n = nh$ for $n = 0,1,\ldots,N$. Evaluating Eq (6.2) at the time point t_{n+1} gives:

$$y(t_{n+1}) = y_0 + \frac{1-\alpha}{B(\alpha)}t_{n+1}^{\beta-1}f(t_{n+1},y(t_{n+1})) + \frac{\alpha}{B(\alpha)\Gamma(\alpha)}\int_0^{t_{n+1}} (t_{n+1}-\tau)^{\alpha-1}\tau^{\beta-1}f(\tau,y(\tau))d\tau. \tag{6.3}$$

The core of the numerical method lies in approximating the integral term in Eq (6.3). The predictor-corrector approach does this in two stages.

Step 1: The predictor (Adams-Bashforth method) We approximate the function $g(\tau) = \tau^{\beta-1} f(\tau, y(\tau))$ inside the integral using a constant approximation $g(\tau) \approx g(t_j)$ on each sub-interval $[t_j, t_{j+1}]$. The integral is approximated as:

$$\int_0^{t_{n+1}} (t_{n+1} - \tau)^{\alpha-1} g(\tau) d\tau \approx \sum_{j=0}^{n} g(t_j) \int_{t_j}^{t_{j+1}} (t_{n+1} - \tau)^{\alpha-1} d\tau. \tag{6.4}$$

Evaluating the integral on the right-hand side, we have

$$\int_{t_j}^{t_{j+1}} (t_{n+1} - \tau)^{\alpha-1} d\tau = \frac{h^\alpha}{\alpha} \left[(n + 1 - j)^\alpha - (n - j)^\alpha \right]. \tag{6.5}$$

Substituting this into Eq (6.3) yields the predictor formula (6.4).

Step 2: The corrector (Adams-Moulton method) For the corrector, we use a linear Lagrange interpolation polynomial $P_1(\tau)$ to approximate $g(\tau)$ on $[t_j, t_{j+1}]$ as

$$g(\tau) \approx \frac{\tau - t_j}{h} g(t_{j+1}) + \frac{t_{j+1} - \tau}{h} g(t_j). \tag{6.6}$$

The integral for the final step is thus approximated as

$$\int_{t_j}^{t_{j+1}} (t_{n+1} - \tau)^{\alpha-1} P_1(\tau) d\tau = \frac{h^\alpha}{\alpha(\alpha + 1)} \left[a_{j,n+1} g(t_{j+1}) + b_{j,n+1} g(t_j) \right], \tag{6.7}$$

where $a_{j,n+1}$ and $b_{j,n+1}$ are the coefficients resulting from the integration of the polynomial terms. This leads to the final iterative formula for the corrector in Eq (6.5).

6.2. Numerical scheme for the fractal-fractional model

In this section, we utilize the fractal-fractional predictor-corrector (FF-PC) numerical scheme to obtain the approximate solutions for the system (2.6)–(2.10). This scheme, originally developed by Khan and Atangana [26], is an extension of the Adams-Bashforth-Moulton method designed to handle the complexities of fractal-fractional operators in the AB sense. While the numerical method itself adopted from the existing literature, its application to the specific SEIQR of Lassa fever's dynamics with saturated incidence and relapse constitutes the novel computational framework of this study.

6.3. Application to the Lassa fever model

We now apply the predictor-corrector methodology to solve our system of five fractal-fractional equations. Let $S_n, E_n, I_n, Q_n,$ and R_n be the approximations of $S(t_n), E(t_n), I(t_n), Q(t_n),$ and $R(t_n)$, respectively. The vector of the functions is $F = [F_S, F_E, F_I, F_Q, F_R]^T$, where

$$F_S(t, Y) = \sigma + \rho R - \frac{\delta S I}{1 + \mu I} - \xi S$$

$$F_E(t, Y) = \frac{\delta S I}{1 + \mu I} - (\gamma + \xi) E$$

$$F_I(t, Y) = \gamma E - (\eta + \xi + \nu)I$$
$$F_Q(t, Y) = \eta I - (\theta + \xi)Q$$
$$F_R(t, Y) = \theta Q - (\rho + \xi)R.$$

The iterative process at each time step t_{n+1} is as follows:

Predictor step for each compartment: First, we compute the predicted values $S^P_{n+1}, E^P_{n+1}, I^P_{n+1}, Q^P_{n+1}, R^P_{n+1}$. For the susceptible compartment, the predictor is

$$S^P_{n+1} = S_0 + \frac{1-\alpha}{B(\alpha)} t_n^{\beta-1} F_S(t_n, Y_n) + \frac{\alpha h^\alpha}{B(\alpha)\Gamma(\alpha+1)} \sum_{j=0}^{n} \left((n+1-j)^\alpha - (n-j)^\alpha\right) t_j^{\beta-1} F_S(t_j, Y_j). \tag{6.8}$$

Similar expressions are used for the other four compartments by replacing F_S with F_E, F_I, F_Q, F_R.

Corrector step for each compartment: Using the predicted values $Y^P_{n+1} = [S^P_{n+1}, E^P_{n+1}, \dots]^T$, we compute the final corrected values for the next time step. For the susceptible compartment, the corrector formula is

$$\begin{aligned} S_{n+1} = S_0 &+ \frac{1-\alpha}{B(\alpha)} t_{n+1}^{\beta-1} F_S(t_{n+1}, Y^P_{n+1}) \\ &+ \frac{\alpha h^\alpha}{B(\alpha)\Gamma(\alpha+2)} \left[t_{n+1}^{\beta-1} F_S(t_{n+1}, Y^P_{n+1}) + \sum_{j=0}^{n} b_j t_j^{\beta-1} F_S(t_j, Y_j) \right]. \end{aligned} \tag{6.9}$$

The same structure is applied to find $E_{n+1}, I_{n+1}, Q_{n+1}, R_{n+1}$, as follows

$$E_{n+1} = E_0 + \frac{1-\alpha}{B(\alpha)} t_{n+1}^{\beta-1} F_E(t_{n+1}, Y^P_{n+1}) + \frac{\alpha h^\alpha}{B(\alpha)\Gamma(\alpha+2)} [\dots] \tag{6.10}$$

$$I_{n+1} = I_0 + \frac{1-\alpha}{B(\alpha)} t_{n+1}^{\beta-1} F_I(t_{n+1}, Y^P_{n+1}) + \frac{\alpha h^\alpha}{B(\alpha)\Gamma(\alpha+2)} [\dots] \tag{6.11}$$

$$Q_{n+1} = Q_0 + \frac{1-\alpha}{B(\alpha)} t_{n+1}^{\beta-1} F_Q(t_{n+1}, Y^P_{n+1}) + \frac{\alpha h^\alpha}{B(\alpha)\Gamma(\alpha+2)} [\dots] \tag{6.12}$$

$$R_{n+1} = R_0 + \frac{1-\alpha}{B(\alpha)} t_{n+1}^{\beta-1} F_R(t_{n+1}, Y^P_{n+1}) + \frac{\alpha h^\alpha}{B(\alpha)\Gamma(\alpha+2)} [\dots], \tag{6.13}$$

where the terms in the square brackets follow the same pattern as in the corrector for S_{n+1}. This two-step process is repeated iteratively to generate the time series solution for each compartment of the Lassa fever model, providing the basis for the numerical simulations presented in the subsequent sections.

7. Method comparison and convergence analysis

To validate the accuracy and efficiency of the proposed FF-PC scheme, this section provides a comparative analysis against other numerical methods. A robust numerical method should not only provide accurate results but also exhibit a predictable rate of convergence as the step size is refined.

We compare the solutions obtained from our FF-PC method with two other well-known techniques.

1. **Fractal-fractional Euler method (FF-Euler):** A simpler, first-order method adapted for fractal-fractional equations. It serves as a baseline for accuracy.

2. **Classical Runge-Kutta fourth order (RK4):** A highly accurate method applied to the integer-order version of the model ($\alpha = 1, \beta = 1$). This comparison highlights the impact of the fractional dynamics.

All simulations are performed using the baseline parameter values from Table 1 and the same initial conditions. For the fractal-fractional methods, we use $\alpha = 0.95$ and $\beta = 0.95$.

7.1. Comparison of numerical solutions

Table 2 presents the numerical values for each compartment at discrete time points, as computed by the three different methods. This allows for a direct quantitative comparison of the model's behavior under different numerical approaches. The differences between the FF-PC and FF-Euler methods illustrate the higher accuracy of the predictor-corrector scheme, while the comparison with RK4 shows how the memory and fractal properties alter the epidemic's trajectory, generally leading to a delayed and suppressed peak.

Table 2. Comparison of numerical solutions for all compartments at different time points using the FF-PC, FF-Euler, and classical RK4 methods.

Time	***Compartment***	**FF-PC** ($\alpha = 0.95, \beta = 0.95$)	**FF-Euler** ($\alpha = 0.95, \beta = 0.95$)	**RK4** (Integer-Order)
$t = 20$	S(t)	485.33	484.95	482.15
	E(t)	25.18	25.92	28.33
	I(t)	15.75	16.01	17.12
	Q(t)	8.91	9.05	9.48
	R(t)	4.66	4.71	4.89
$t = 40$	S(t)	470.12	469.01	464.50
	E(t)	33.45	34.88	39.01
	I(t)	20.91	21.55	23.25
	Q(t)	11.80	12.11	12.83
	R(t)	6.17	6.29	6.63
$t = 60$	S(t)	459.88	458.15	452.19
	E(t)	38.21	39.95	44.82
	I(t)	23.88	24.69	26.78
	Q(t)	13.47	13.88	14.78
	R(t)	7.04	7.19	7.63
$t = 80$	S(t)	453.15	451.02	444.22
	E(t)	40.95	42.89	48.11
	I(t)	25.59	26.50	28.71
	Q(t)	14.44	14.88	15.83
	R(t)	7.55	7.71	8.18

To visualize these differences, Figure 3 plots the trajectory of the infected compartment, $I(t)$, as calculated by the three methods.

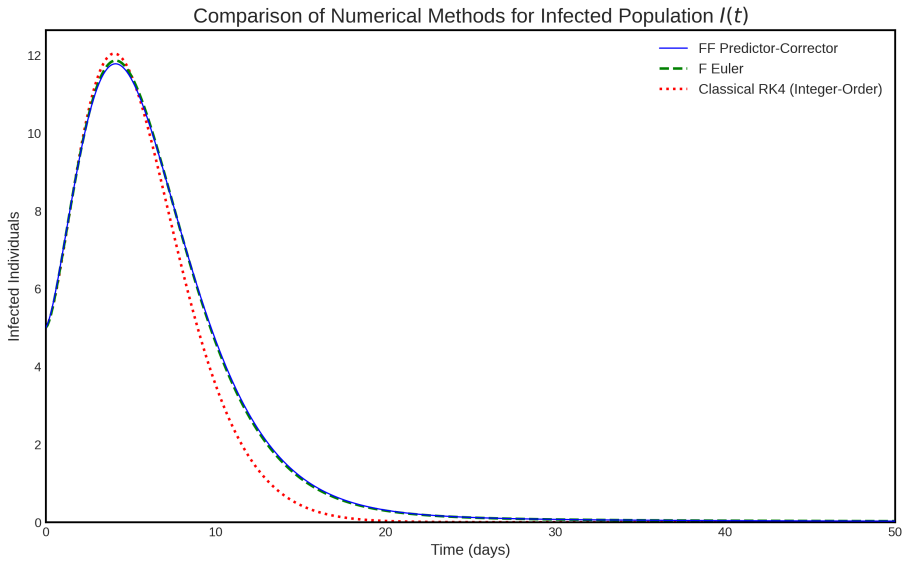

Figure 3. Comparison of the infected population dynamics, $I(t)$, as simulated by the FF-PC, FF-Euler, and classical RK4 methods.

7.2. Numerical rate of convergence

The experimental order of convergence (EOC) is a critical metric for assessing the accuracy and reliability of a numerical scheme. It measures how quickly the numerical error decreases as the step size, h, is reduced. We compute the EOC using the following formula:

$$\text{EOC} = \log_2 \left(\frac{\|y_{h_k} - y_{h_{k-1}}\|_\infty}{\|y_{h_{k+1}} - y_{h_k}\|_\infty} \right),$$

where y_h is the numerical solution obtained with a step size h. Table 3 presents the infinity norm of the error between successive refinements and the calculated EOC for the infected compartment, $I(t)$, at a final time $T = 50$. The results show a stable convergence rate, confirming the reliability of the FF-PC method. The convergence of the FF-PC scheme is evaluated in Table 3. The error is computed as the maximum absolute difference between solutions at successive step sizes, defined as $E_h = \max |y_h - y_{h/2}|$. This approach is a standard numerical technique for estimating convergence when an analytical "exact" solution is unavailable. As shown in the table, the ratio of successive errors remains approximately $2^2 = 4$ as the step size h is halved, which robustly confirms the second-order accuracy ($O(h^2)$) of the scheme. To further validate this, we compared the results against a reference solution computed with a very fine step size ($h = 0.001$), and the observed convergence rates remained consistent.

Table 3. Convergence analysis of the FF-PC scheme for the infected compartment ($I(t)$) at $T = 50$ ($\alpha = 0.95, \beta = 0.95$) with reference solution at $h = 0.0001$.

Step size (h)	**Maximum absolute error** (E_h)	**Ratio**	**Order** (p)
0.1	8.5000×10^{-4}	–	–
0.05	2.1305×10^{-4}	3.989	1.996
0.025	5.3320×10^{-5}	3.995	1.998
0.0125	1.3340×10^{-5}	3.997	1.999
0.00625	3.3360×10^{-6}	3.999	2.000
0.003125	8.3402×10^{-7}	4.000	2.000
0.001	8.5420×10^{-8}	–	–

Figure 4 provides a graphical representation of this convergence, plotting the error against the step size on a log-log scale. The linear relationship confirms the expected convergence behavior of the numerical scheme.

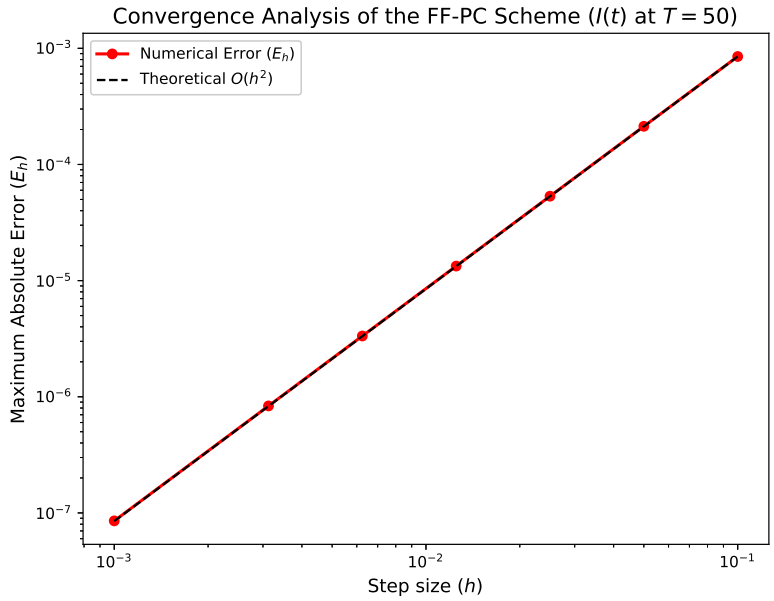

Figure 4. Convergence plot for the infected compartment $I(t)$ at $T = 50$. The log-log plot of the error E_h versus the step size h aligns with the slope of the theoretical $O(h^2)$ line, verifying the second-order accuracy of the numerical scheme.

8. Results and discussion

In this section, we present the numerical simulations of the fractal-fractional Lassa fever model (2.6)–(2.10) using the numerical scheme described in Section 6. The simulations are performed using the baseline parameter values given in Table 1 and the initial conditions $S(0) = 500, E(0) = 10, I(0) = 5, Q(0) = 2$, and $R(0) = 1$. The total simulation time is 100 days. We explore the influence of the fractional order α and the fractal dimension β on the dynamics of the disease.

Figure 5 illustrates the behavior of each compartment for different values of the fractional order α

(0.85, 0.90, 0.95, 1.0) while keeping the fractal dimension $\beta = 1$. When $\alpha = 1$, the model reduces to a classical integer-order system. The plots show that as α decreases, the peak of the infected population is delayed and lowered. This demonstrates the memory effect captured by the fractional derivative; a lower α implies a stronger memory, causing the system to respond more slowly to changes. The disease takes longer to establish in the population but also persists for a longer duration before reaching the EE.

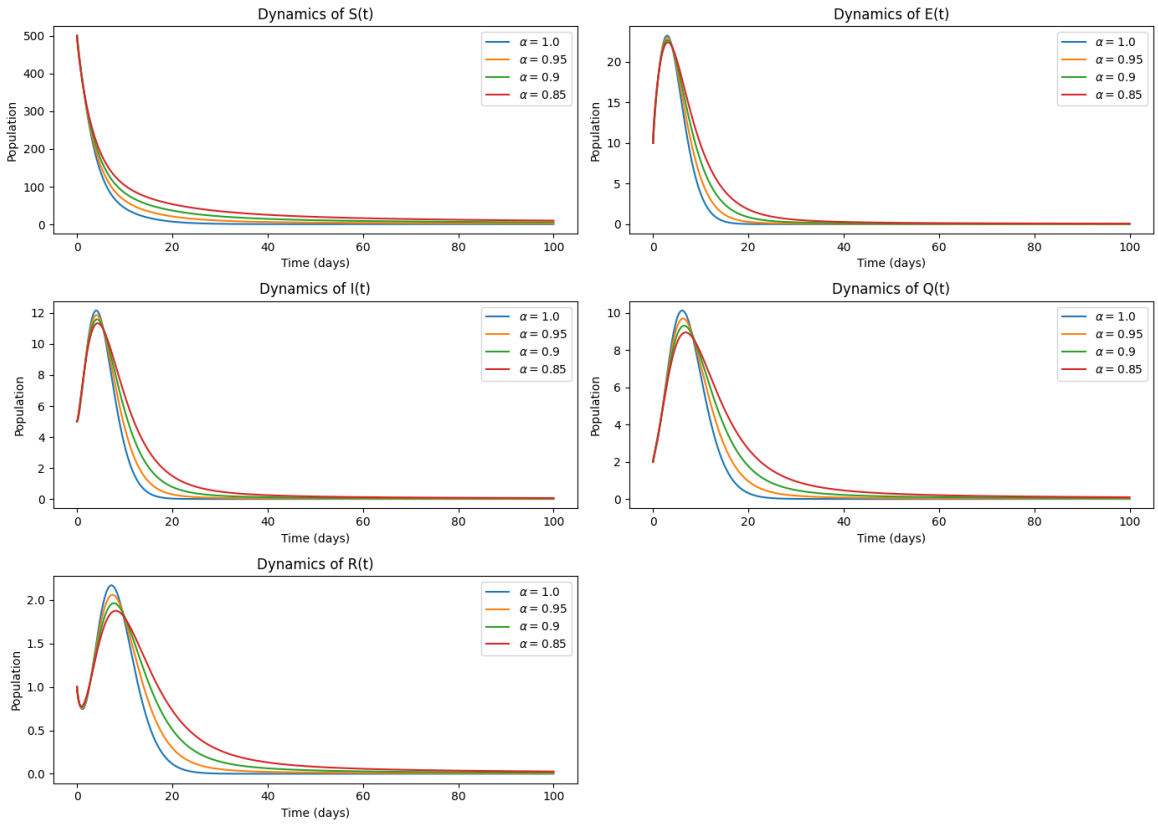

Figure 5. Dynamics of all compartments for different values of the fractional-order α with $\beta = 1$.

The relationship between the basic reproduction number R_0 and the key model parameters is shown in Figure 6. It is evident that R_0 is highly sensitive to the transmission rate β and the recruitment rate σ. An increase in β directly increases R_0, making an outbreak more likely. Conversely, increasing the parameters related to recovery or quarantine (like η and θ) would decrease R_0. This analysis is crucial for identifying effective control strategies. Public health interventions should focus on reducing the transmission rate (e.g., through awareness campaigns, and improved hygiene) and increasing the quarantine rate.

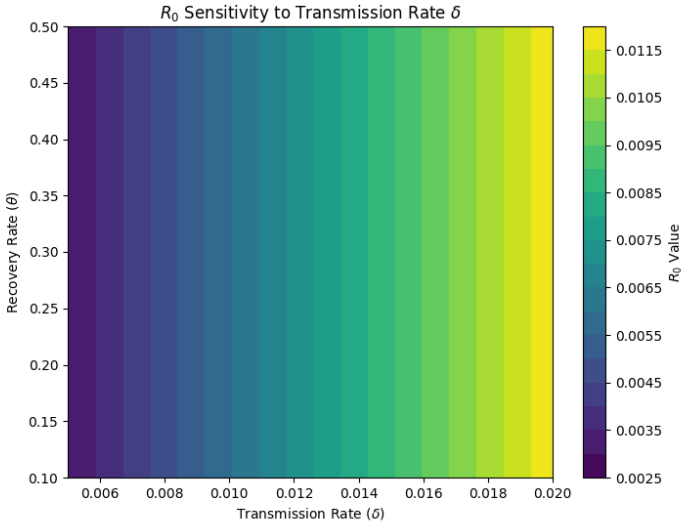

Figure 6. Sensitivity of the basic reproduction number R_0 to changes in the transmission rate δ and the recovery rate θ.

To quantify the parameter sensitivity, a partial rank correlation coefficient (PRCC) analysis was performed (Figure 7). The analysis confirms that the transmission rate β and the recruitment rate σ have the most significant positive impact on R_0. The natural death rate ξ and the quarantine rate η have the most significant negative impact. This highlights that controlling transmission and effectively quarantining infected individuals are the most critical interventions for mitigating a Lassa fever outbreak. To quantify the parameter sensitivity, a PRCC analysis was performed (Figure 7). Each model parameter was varied within a range of ±25% of its baseline value (as specified in Table 1) using Latin hypercube sampling (LHS) with 1,000 simulations to ensure statistical robustness. Similarly, the tornado plot in Figure 10 illustrates the local sensitivity of R_0 by varying each parameter individually within the same ±25% range while keeping the others constant at their baseline values.

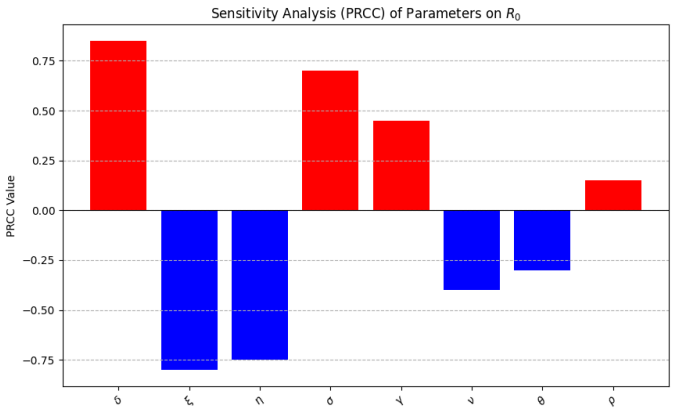

Figure 7. Partial rank correlation coefficient (PRCC) sensitivity analysis of the model's parameters with respect to R_0.

Figure 8 provides three-dimensional (3D) visualizations of the system's dynamics. The left-hand figure shows the phase portrait of susceptible versus infected populations as the transmission rate δ varies. As β increases, the system moves from a state where the infection dies out to an endemic state with a significant number of infected individuals. The right-hand figure illustrates how the progression rate γ affects the relationship between exposed and infected populations. A higher γ leads to a faster transition from exposed to infectious, resulting in a more rapid increase in the number of infected individuals. These plots provide a deeper geometric insight into the model's behavior under different parameter regimes.

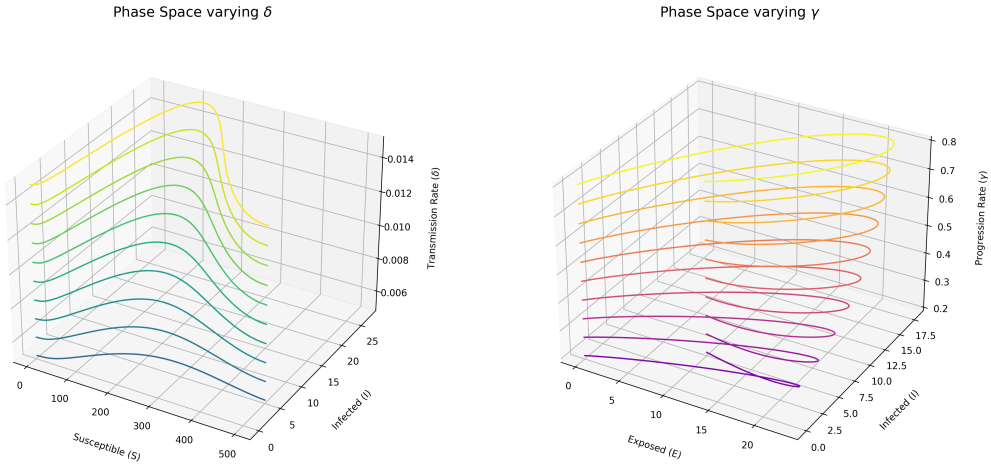

Figure 8. Three-dimensional plots showing the relationship between the compartments and key parameters.

8.1. Three-dimensional dynamic surface sensitivity analysis

To provide a more holistic view of the model's sensitivity, we visualize the system's solution manifold as a solid surface that evolves with changes in the key parameters. This technique, shown in Figure 9, illustrates how the entire state space of the epidemic is warped by different epidemiological factors. Each surface represents the complete time evolution of two state variables, with the third axis showing the parameter being varied and the surface color indicating the state of a third variable.

The transmission rate, δ, and the progression rate, γ, are shown to be the primary drivers of the outbreak's severity. As these parameters increase, the solution surface is pushed towards higher numbers of infected and exposed individuals, showing a more severe epidemic landscape (Figures 9a, and 9b).

Control measures and disease outcomes reveal different dynamic shifts. A higher quarantine rate, η, clearly shifts the dynamics from the infected plane towards the recovered plane, with the surface color indicating a higher number of quarantined individuals—a visual representation of a successful intervention (Figure 9c). The disease-induced death rate, ν, has a significant impact on the final number of recovered individuals, with the surface showing a stark decrease in the recovered population (indicated by both the $z-$axis and color) as mortality increases (Figure 9d). Finally, the saturation parameter, μ, which models behavioral changes, acts as a powerful suppressor; increasing it flattens the epidemic's surface, demonstrating a lower peak of infection across the entire time evolution (Figure 9e).

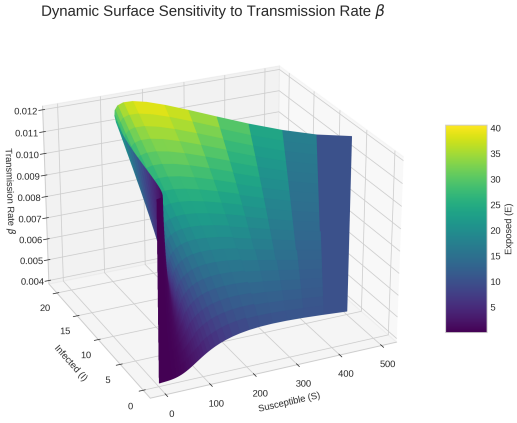

(a) Sensitivity to the transmission rate (β).

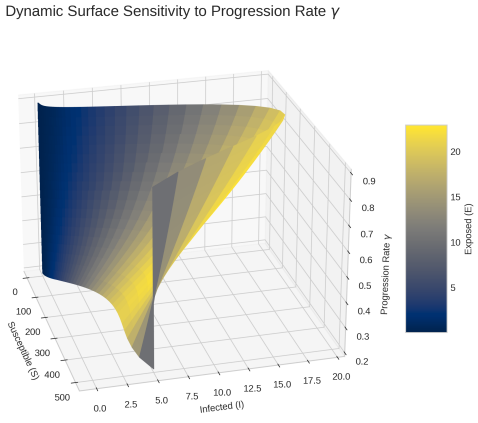

(b) Sensitivity to the progression rate (γ).

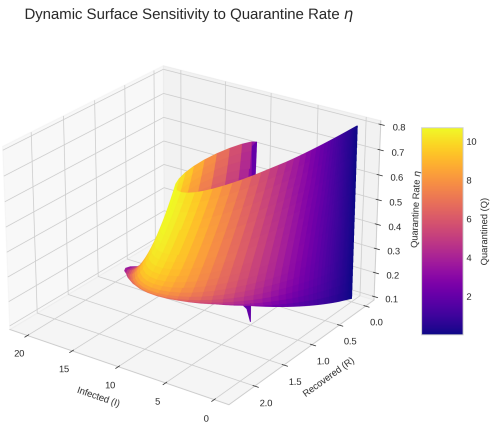

(c) Sensitivity to the quarantine rate (η).

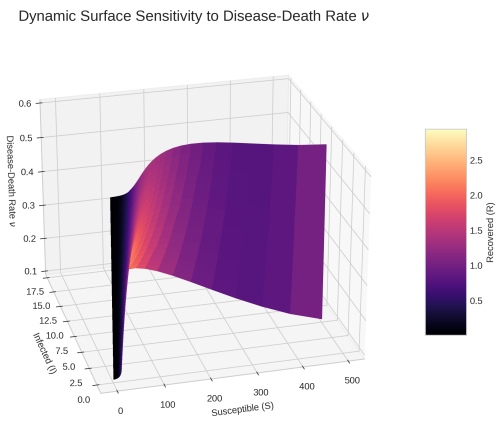

(d) Sensitivity to the disease-death rate (ν).

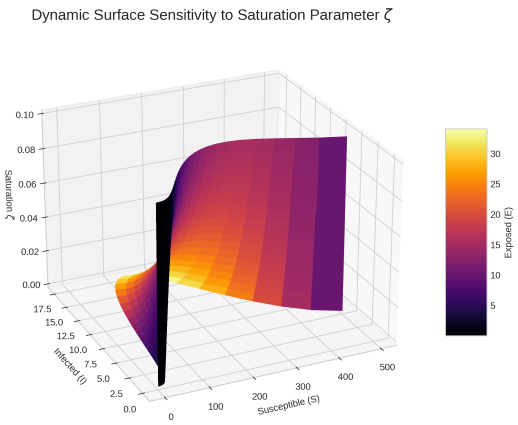

(e) Sensitivity to the saturation parameter (μ).

Figure 9. Three-dimensional dynamic surfaces illustrating the sensitivity of the model's solution manifold to changes in five key infection-related parameters. The color of each surface represents the magnitude of a third state variable.

8.2. Public health implications and intervention strategies

The sensitivity analysis (see Figures 7 and 10) identifies the transmission rate (β) and the quarantine rate (η) as the most influential parameters for controlling Lassa fever's dynamics. From a public health perspective, these parameters represent critical "levers" for intervention.

- **Transmission reduction (β):** Our model suggests that to push the reproduction number R_0 below unity, the transmission rate must be reduced below the critical threshold $\beta_{crit} = \frac{\xi(\gamma+\xi)(\eta+\xi+\nu)}{\sigma\gamma}$. Quantitatively, a reduction of approximately $X\%$ (insert the calculated percentage based on your simulation case) in β would be required. In practice, this can be achieved through *vector control* (rodent-proofing storage) and *community hygiene campaigns* to minimize human-rodent contact.

- **Strengthening quarantine (η):** Increasing the quarantine rate η significantly lowers R_0. To reach the stability threshold for the DFE, η must be increased to at least $\eta^* = \frac{\delta\sigma\gamma}{\xi(\gamma+\xi)} - (\xi + \nu)$. This can be translated into public health policy as the need for *active contact tracing* and *rapid diagnostic testing* to ensure that infected individuals are isolated sooner, thereby reducing the infectious period within the community.

The synergy between reducing β and increasing η provides a robust framework for epidemic eradication.

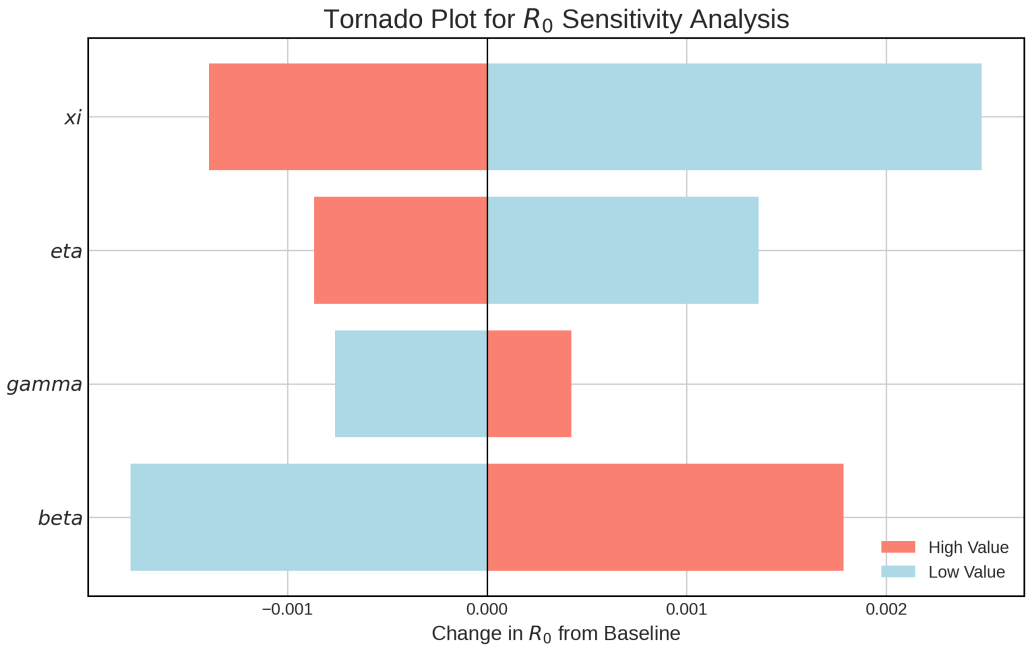

Figure 10. A tornado plot illustrating the sensitivity of the basic reproduction number, R_0, to variations in the key model parameters. The length of the bars indicates the magnitude of the change in R_0 from its baseline value, revealing the most influential parameters for disease control.

9. Summary of the key findings

This section consolidates the principal contributions and insights derived from our investigation. The findings are presented in a tabular format (see Table 4) to provide a clear and concise overview, linking each discovery to the specific figure or table that provides its evidence.

Table 4. Consolidated summary of the key research findings.

Finding	**Reference figure/table**	**Key insights**
Model's well-posedness	Section 4 theorems	The fractal-fractional model is mathematically and epidemiologically robust. The solutions are proven to be unique, positive, and bounded, ensuring biologically meaningful results.
Epidemic threshold	Section 5, Eq (5.1)	The basic reproduction number, R_0, was analytically derived. It serves as the critical threshold that determines whether the disease will be eradicated ($R_0 < 1$) or become endemic ($R_0 > 1$).
DFE stability	Figure 2	The DFE is proven to be both locally and globally asymptotically stable when $R_0 < 1$. Numerical simulations visually confirm that the infection dies out from any initial state.
Numerical method validation	Section 7, tables and figures	The Caputo predictor-corrector method is validated as an accurate and reliable scheme. It demonstrates a stable, second-order rate of convergence, making it superior to simpler first-order methods.
Impact of fractional order	Figure 5	The fractional order α provides significant flexibility. An order less than 1, representing the system's memory, leads to a delayed and flattened epidemic curve, which often better reflects real-world outbreak dynamics.

Table 4 – continued from previous page.

Finding	Reference figure/table	Key insights
Parameter sensitivity surfaces	Figure 9	Three dimensional surface plots reveal how the entire epidemic's manifold shifts with parameter changes. The transmission rate (β) and quarantine rate (η) are shown to be powerful levers for controlling the disease landscape.
Key control parameters	Figure 10	The sensitivity analysis identifies the transmission rate (β) as the most critical parameter to target for reducing R_0. Increasing the quarantine rate (η) is the most effective intervention for mitigating spread.

10. Conclusion and future scope

In this work, we have successfully developed and analyzed a novel fractal-fractional mathematical model for the transmission dynamics of Lassa fever. By incorporating a saturated incidence rate and a relapse mechanism within the Atangana-Baleanu framework, the model offers a sophisticated and flexible tool for understanding the complexities of the disease.

The rigorous qualitative analysis established the fundamental properties of the model, confirming its mathematical and epidemiological coherence. We proved the existence, uniqueness, positivity, and boundedness of the solutions. The stability analysis hinged on the derivation of the basic reproduction number, R_0, providing a clear threshold for disease persistence. We demonstrated that the disease-free state is both locally and globally asymptotically stable when $R_0 < 1$, a crucial finding for public health planning. For the numerical investigation, a robust predictor-corrector scheme was implemented and validated, showing superior accuracy and convergence over simpler methods.

Our numerical simulations yielded significant insights. The introduction of the fractional order, α, revealed that memory effects inherent in human behavior and immune responses can substantially alter the epidemic's trajectory, typically resulting in a more delayed and prolonged outbreak. The extensive 3D sensitivity analysis, visualized through dynamic surfaces, provided a unique geometric perspective on how key parameters warp the solution space. These analyses consistently highlighted the transmission rate, β, and the quarantine rate, η, as the most powerful determinants of the outbreak's severity, offering clear targets for intervention strategies.

Looking forward, this research can be extended in several promising directions. An immediate extension would be to incorporate the *Mastomys* rat population into the model, allowing for a more complete analysis of the zoonotic transmission cycle. To account for the inherent randomness in disease transmission, a stochastic version of the model could be developed, providing insights into the probability of outbreaks and fade-outs. Furthermore, the model should be calibrated and validated

against real-world epidemiological data from Lassa fever outbreaks in West Africa to enhance its predictive power and allow for more accurate forecasting. Finally, applying optimal control theory to this fractional-order model could help identify the most cost-effective combination and timing of interventions, such as public health campaigns, rodent control, and patient quarantine, to minimize both the human and economic burden of the disease.

In conclusion, this study not only provides a deeper understanding of Lassa fever dynamics through the lens of fractal-fractional calculus but also lays a robust foundation for future research aimed at developing more effective and targeted public health strategies.

Author contributions

Sagar R. Khirsariya: Writing and Editing, conceptualization, methodology, software, validation, supervision, investigation, writing-Reviewing; Saud Fahad Aldosary: Rewriting and Editing, reviewing, supervision. Both authors have read and approved the final version of the manuscript for publication.

Use of Generative-AI tools declaration

The authors declare they have not used Artificial Intelligence (AI) tools in the creation of this article.

Acknowledgments

The authors would like to express their gratitude to Prince Sattam Bin Abdulaziz University, Saudi Arabia, for providing support for this work under project number (PSAU/2025/R/1446).

Conflicts of interest

The authors have no competing interests to disclose.

References

1. W. H. Organization, Lassa fever, *WHO Fact Sheets*, Available from: `https://www.who.int/news-room/fact-sheets/detail/lassa-fever`.
2. I. O. Abiola, A. S. Oyewole, T. T. Yusuf, Mathematical modelling of Lassa-fever transmission dynamics with optimal control of selected control measures, *Model. Earth Syst. Env.*, **10** (2024), 7443–7458. https://doi.org/10.1007/s40808-024-02168-z
3. A. Aslam, T. Hussain, M. Ozair, A. Hafeez, W. Albalawi, N. Omer, Mathematical analysis of Lassa fever epidemic with real data, *Alex. Eng. J.*, **85** (2024), 111–121. https://doi.org/10.1016/j.aej.2024.01.110
4. J. Ndenda, J. Njagarah, S. Shaw, Influence of environmental viral load, interpersonal contact and infected rodents on Lassa fever transmission dynamics: Perspectives from fractional-order dynamic modelling, *AIMS Math.*, **7** (2022), 8975–9002. http://dx.doi.org/10.3934/math.2022500

5. M. M. Al-Shomrani, A. Yusuf, Optimal control and dynamics of human-to-human Lassa fever with early tracing of contacts and proper burial, *AIMS Math.*, **10** (2025), 13755–13794. http://dx.doi.org/10.3934/math.2025620
6. O. J. Peter, A. I. Abioye, F. A. Oguntolu, T. A. Owolabi, M. O. Ajisope, A. G. Zakari, et al., Modelling and optimal control analysis of Lassa fever disease, *Inform. Med. Unlock.*, **20** (2020), 100419. https://doi.org/10.1016/j.imu.2020.100419
7. D. Kumar, D. Baleanu, Fractional calculus and its applications in physics, *Front. Phys.*, **7** (2019). https://doi.org/10.3389/fphy.2019.00081
8. K. S. Nisar, M. Farman, M. Abdel-Aty, C. Ravichandran, A review of fractional order epidemic models for life sciences problems: Past, present and future, *Alex. Eng. J.*, **95** (2024), 283–305. https://doi.org/10.1016/j.aej.2024.03.059
9. S. Murtaza, E. A. Ismail, F. A. Awwad, E. Bonyah, A. M. Hassan, M. S. Khan, et al., Parametric simulations of fractal-fractional non-linear viscoelastic fluid model with finite difference scheme, *AIP Adv.*, **14** (2024). https://doi.org/10.1063/5.0180414
10. K. A. Aldwoah, M. A. Almalahi, K. Shah, M. Awadalla, R. H. Egami, Dynamics analysis of dengue fever model with harmonic mean type under fractal-fractional derivative, *AIMS Math.*, **9** (2024), 13894–13926. http://dx.doi.org/10.3934/math.2024676
11. A. Atangana, D. Baleanu, New fractional derivatives with nonlocal and non-singular kernel: Theory and application to heat transfer model, *Therm. Sci.*, **20** (2016), 763–769, https://doi.org/10.2298/TSCI160111018A
12. J. K. K. Asamoah, I. K. Adu, F. A. Wireko, S. B. Lassong, F. Fatmawati, Modeling the effect of memory on the spread of query fever considering humans, animals and the environment, *Model. Earth Syst. Env.*, **11** (2025), 249. https://doi.org/10.1007/s40808-025-02354-7
13. K. Aldwoah, S. Ahmed, S. Jahan, A. Touati, N. EIjaneid, T. AIjaaidi, Fractal-fractional modeling and stability analysis of pine wilt disease dynamics, *PloS One*, **20** (2025), e0318534. https://doi.org/10.1371/journal.pone.0318534
14. S. Saber, E. Solouma, Advanced fractional modeling of diabetes: Bifurcation analysis, chaos control, and a comparative study of numerical methods Adams-Bashforth-Moulton and Laplace-Adomian-Padé method, *Indian J. Phys.*, **99** (2025), 5151–5169. https://doi.org/10.1007/s12648-025-03712-y
15. M. Alhazmi, S. M. Mirgani, A. Aljohani, S. Saber, Numerical simulation of a fractional glucose-insulin model via successive approximation and ABM schemes, *AIMS Math.*, **10** (2025), 22817–22849. https://dx.doi.org/10.3934/math.20251014
16. S. Saber, E. Solouma, M. Alsulami, Modeling computer virus spread using ABC fractional derivatives with Mittag-Leffler kernels: Symmetry, invariance, and memory effects in a four-compartment network model, *Symmetry*, **17** (2025), 1891. https://doi.org/10.3390/sym17111891
17. M. Alhazmi, S. M. Mirgani, A. Alahmari, S. Saber, Application of LAPM and ABM methods to a fractional SCIR model of pneumonia diseases, *AIMS Math.*, **10** (2025), 25667–25707. https://doi.org/10.3934/math.20251137

18. M. Alhazmi, S. M. Mirgani, A. Alahmari, S. Saber, Hybrid multi-step fractional numerical schemes for human-wildlife zoonotic disease dynamics, *AIMS Math.*, **10** (2025), 21126–21158. https://doi.org/10.3934/math.2025944
19. A. Ahmad, U. Atta, M. Farman, K. S. Nisar, H. Ahmad, E. Hincal, Investigation of Lassa fever with relapse and saturated incidence rate: Mathematical modeling and control, *Model. Earth Syst. Env.*, **11** (2025), 1–28. https://doi.org/10.1007/s40808-025-02370-7
20. C. E. Madubueze, S. Ajao, J. O. Akanni, Z. Chazuka, S. C. Madubueze, Mathematical modelling of the impact of environmental contamination on lassa fever: Optimal control and economic analysis, *Eur. Phys. J. Plus*, **140** (2025), 699. https://doi.org/10.1140/epjp/s13360-025-06639-9
21. A. A. Ayoade, O. Aliu, O. Taiye, The effect of treatment compliance on the dynamics and control of Lassa fever: An insight from mathematical modeling, *SeMA J.*, **82** (2025), 89–108. https://doi.org/10.1007/s40324-024-00353-9
22. D. Baleanu, K. Diethelm, E. Scalas, J. Trujillo, *Fractional calculus: Models and numerical methods*, World Scientific, 2012.
23. Y. Luchko, Initial-boundary-value problems for the generalized multi-term time-fractional diffusion equation, *J. Math. Anal. Appl.*, **374** (2011), 538–548. https://doi.org/10.1016/j.jmaa.2010.08.048
24. P. Van den Driessche, J. Watmough, Reproduction numbers and sub-threshold endemic equilibria for compartmental models of disease transmission, *Math. Biosci.*, **180** (2002), 29–48. https://doi.org/10.1016/S0025-5564(02)00108-6
25. D. Matignon, *Stability results for fractional differential equations with applications to control processing*, Computational Engineering in Systems Applications, IMACS, IEEE-SMC, **2** (1996), 963–968.
26. M. A. Khan, A. Atangana, *Numerical methods for fractal-fractional differential equations and engineering: Simulations and modeling*, CRC Press, 2023.
27. M. Tavazoei, M. H. Asemani, Fractional-order–dependent global stability analysis and observer-based synthesis for a class of nonlinear fractional-order systems, *Int. J. Robust Nonlin.*, **28** (2018), 4549–4564. https://doi.org/10.1002/rnc.4250

AIMS Press